Effective two-phase flow in heterogeneous media under temporal pressure fluctuations

Diogo Bolster,[1] Marco Dentz,[1] and Jesus Carrera[2]

Received 17 September 2008; revised 11 February 2009; accepted 20 February 2009; published 9 May 2009.

[1] We study the combined effect of spatial heterogeneity and temporal pressure fluctuations on the dispersion of the saturation of a displacing fluid during injection into an immiscible one. In a stochastic modeling framework, we define two different dispersion quantities, one which measures the front uncertainty due to temporal pressure fluctuations and another one which quantifies the actual spreading and dispersion of the saturation front in a typical medium realization. We derive an effective large-scale flow equation for the saturation of the displacing fluid that is characterized by a nonlocal dispersive flux term. From the latter we derive measures for the spread of the saturation front due to spatiotemporal fluctuations. Our analysis demonstrates that temporal fluctuations enhance the front uncertainty but not the average spreading of the saturation front. The analytical developments are complemented by numerical simulations of the full two-phase flow problem. Correct assessment of the spread of the saturation front is of importance to several applications, including the assessment of the sequestration potential of a carbon dioxide storage site, for example. Spreading enhances the surface area between the fluids, which in turn enhances the dissolution and entrapment efficiency. The latter facilitates reactions and thus the sequestration of CO_2 in stable forms. Our study provides a theoretical basis for the design of injection strategies to optimize dispersion and to minimize uncertainty of the saturation front.

Citation: Bolster, D., M. Dentz, and J. Carrera (2009), Effective two-phase flow in heterogeneous media under temporal pressure fluctuations, *Water Resour. Res.*, *45*, W05408, doi:10.1029/2008WR007460.

1. Introduction

[2] The injection of one fluid into another in geological porous media is one of great interest in the fields of petroleum engineering [*Lake*, 1989], gas storage and more recently, with the ever increasing awareness of climate change, the sequestration of anthropogenic CO_2 in deep saline aquifers [*Bachu*, 2000]. The study of such flows requires a multiphase modeling approach and a manner to study this is to manipulate the mass balance equations of the individual phases in such a manner as to write governing equations that look similar to advection-dispersion equations for single phase flows. According to *Bear* [1972], a multiphase flow problem can be cast into an equation that looks much like an advection-dispersion type equation for the saturation $S(\mathbf{x}, t)$ of an immiscible fluid such that

$$\frac{\partial S(\mathbf{x},t)}{\partial t} + \mathbf{v}[\mathbf{x}, S(\mathbf{x},t)] \cdot \nabla S(\mathbf{x},t) + \nabla \cdot D[\mathbf{x}, S(\mathbf{x},t)] \nabla S(\mathbf{x},t) = 0. \quad (1)$$

[3] Note that the latter is highly nonlinear as the drift $\mathbf{v}$ as well as the dispersion coefficient D depend on the saturation $S(\mathbf{x}, t)$ via the dependence of capillary pressure and relative permeability on saturation as will be outlined below. While (1) has the appearance of an advection-diffusion equation caution must be taken with this analogy as the nonlinearities can lead to behavior that is very different from the traditional linear advection diffusion equation used for solute transport.

[4] Multiphase flow in homogeneous porous media has been studied extensively over the years [*Marle*, 1981, and references therein]. However, in most geological porous media the properties of the medium, such as the permeability, fluctuate over a large range of values. From a practical perspective it is desirable to describe the flow through such a medium on a large scale, which requires a qualitative and quantitative understanding of the impact of small-scale heterogeneities and temporal pressure fluctuations on the effective flow behavior. While it is not necessarily possible to resolve the full medium heterogeneity on all scales, it is not generally necessary to do so as we are typically seeking an integral understanding of the system behavior on a large scale. Stochastic modeling [e.g., *Dagan*, 1989; *Gelhar*, 1993] provides an efficient and systematic framework to integrate spatiotemporal fluctuations into an effective flow description and to assess fluctuation-induced uncertainties of the large-scale system characteristics. With this approach the permeability field is modeled as a typical realization of an (ergodic) correlated spatial random process and temporal pressure fluctuations are modeled as an (ergodic) correlated temporal random process [e.g., *Dentz and Carrera*, 2003]. The results presented herein are readily extendable to

[1]Department of Geotechnical Engineering and Geosciences, Technical University of Catalonia, Barcelona, Spain.
[2]Institute of Environmental Analysis and Water Studies, CSIC, Barcelona, Spain.

0043-1397/09/2008WR007460$09.00

periodic fluctuation patterns too. The effective flow behavior can then be determined by averaging of all possible realizations of the respective ensembles [e.g., *Tartakovsky and Neuman*, 1998b, 1998a]. It is often tacitly assumed that the ensemble averaged flow parameters are representative of the effective large-scale behavior within a single realization. This, however, is not self-evident. The physical meaning of large-scale coefficients depends intrinsically on how they are defined as an ensemble average.

[5] Many multiphase flow processes, including the aforementioned oil displacement and carbon sequestration problems, are modeled as ideal displacements, which consist of one fluid displacing another immiscible one. In these applications quantifying the spread of the saturation front due to heterogeneities can be an important task. In order to optimize oil recovery one may want to minimize such spreading effects, while for the geological sequestration of CO_2 it may be desirable to maximize the surface area between the CO_2 and the host fluid in order to increase dissolution and entrapment of CO_2, thus enhancing sequestration efficiency.

[6] For the case of single phase solute transport it is well known that the heterogeneities lead to a heterogeneous flow path structure, resulting in greater travel distances along one path compared to another [e.g., *Kitanidis*, 1988; *Dentz et al.*, 2000; *Fiori*, 2001; *Cirpka and Attinger*, 2003; *Dentz and Carrera*, 2003]. This results in greater mixing on the macroscale, which can be captured by a macrodispersion term [e.g., *Gelhar and Axness*, 1983; *Dagan*, 1989]. Because of the formal similarity of the advection-dispersion equation for the transport of a solute and the nonlinear advection-dispersion type equation (1) for the saturation one might expect a similar mixing effect by the heterogeneities in an immiscible displacement flow. As the two fluids are immiscible, macrodispersion here does not reflect physical mixing, but rather a spreading of the saturation distribution.

[7] *Langlo and Espedal* [1995] explicitly determined a macrodispersion coefficient that models the dispersive flux in an effective equation for the saturation of the wetting phase in immiscible two-phase flow. They used a perturbation approach in flow scenarios with and without capillary forces. Their result for the macrodispersion coefficient is similar to the one obtained for heterogeneity-induced solute spreading in single phase flow.

[8] *Cvetkovic and Dagan* [1996] studied this macrodispersion effect in an immiscible flow scenario using the Buckley-Leverett approximation, i.e., disregarding capillary pressure and gravity. Applying a Lagrangian perturbation approach they found a dispersive large-scale effect, which, however, is not explicitly determined.

[9] *Neuweiler et al.* [2003] used a perturbation theory approach in order to determine a large-scale mixing parameter for the displacing fluid for the flow problem in a two dimensional heterogeneous porous medium. They developed an explicit definition of a large-scale mixing coefficient for the nonlinear problem.

[10] *Kinzelbach and Ackerer* [1986] and *Rehfeldt and Gelhar* [1992] pointed out that temporal pressure fluctuations can lead to enhanced solute dispersion in heterogeneous media. *Dentz and Carrera* [2003] and *Cirpka and Attinger* [2003] quantify the interaction of temporal pressure fluctuations and spatial heterogeneity using a perturbation analysis in the fluctuations of the spatial and temporal random fields.

[11] In section 2 we present the mathematical model that we use to study this problem. In section 3 we quantify the impact of medium heterogeneities on the effective large-scale flow behavior, which, using moments, we quantify by a "macrodispersion" coefficient. We also define an ensemble quantity that measures the uncertainty of the saturation front due to spatiotemporal fluctuation. In section 4 we study the problem at hand numerically and quantitatively compare the results.

2. Model

2.1. Two-Phase Flow

[12] The flow of two immiscible fluids in a porous medium is described by the coupled momentum conservation and mass conservation equations. Momentum conservation is expressed by Darcy's law, which reads as [*Bear*, 1972]

$$\mathbf{q}^{(i)}(\mathbf{x},t) = -\frac{k(\mathbf{x})k_{ri}(S_i)}{\mu_i}[\nabla p_i(\mathbf{x},t) + \rho_i g \mathbf{e}_3], \tag{2}$$

where $\mathbf{q}^{(i)}(\mathbf{x}, t)$ and $p_i(\mathbf{x}, t)$ are specific discharge and pressure of fluid i, μ_i and ρ_i are viscosity and density of fluid i, $k(\mathbf{x})$ is the intrinsic permeability of the porous medium, $k_{ri}[S_i(\mathbf{x}, t)]$ is the relative permeability of phase i (which depends on saturation); $\mathbf{e}_3$ denotes the unit vector in 3 direction. Mass conservation for each fluid is given by [*Bear*, 1972]

$$\frac{\partial}{\partial t}\omega\rho_i S_i(\mathbf{x},t) + \nabla\cdot\rho_i\mathbf{q}^{(i)}(\mathbf{x},t) = 0. \tag{3}$$

[13] We assume here that the medium and the fluid are incompressible so that porosity ω and density ρ_i of each fluid are constant. The saturations S_i of each fluid sum up to one and the difference of the pressures in each fluid defines the capillary pressure $p_c(S)$

$$S_1 + S_2 = 1 \tag{4}$$

$$p_1 - p_2 = p_c(S_1), \tag{5}$$

where $i = 1$ indicates the nonwetting fluid. In the following we focus on the saturation of fluid 1 and drop the subscript in the following. From the incompressibility conditions and mass conservation, it follows that the divergence of the total specific discharge $\mathbf{q}(\mathbf{x}, t) = \mathbf{q}^{(1)}(\mathbf{x}, t) + \mathbf{q}^{(2)}(\mathbf{x}, t)$ is zero:

$$\nabla\cdot\mathbf{q}(\mathbf{x},t) = 0. \tag{6}$$

Eliminating $\mathbf{q}^{(1)}(\mathbf{x}, t)$ from equation (3) in favor of $\mathbf{q}(\mathbf{x}, t)$, one obtains [*Bear*, 1972]

$$\begin{aligned}\frac{\partial S(\mathbf{x},t)}{\partial t} &+ \frac{\partial}{\partial S}[\psi(S)(\mathbf{q}(\mathbf{x},t) + k(\mathbf{x})\lambda_2(S)g\Delta\rho\mathbf{e}_3)]\cdot\nabla S(\mathbf{x},t)\\ &+ \psi(S)\lambda_2(S)g\Delta\rho\frac{\partial k(\mathbf{x})}{\partial x_3} - \nabla\\ &\cdot\left[\psi(S)k(\mathbf{x})\lambda_2(S)\frac{\mathrm{d}p_c(S)}{\mathrm{d}S}\nabla S(\mathbf{x},t)\right] = 0,\end{aligned} \tag{7}$$

where $\Delta\rho = \rho_2 - \rho_1$. We set $\omega = 1$ for simplicity (which is equivalent to rescaling time). The fractional flow function $\psi(S)$ is defined by

$$\psi(S) = \frac{\lambda_1(S)}{\lambda_1(S) + \lambda_2(S)}, \tag{8}$$

where the phase mobilities λ_i are defined as the ratio of relative permeability to fluid viscosity, $\lambda_i = k_i(S)/\mu_i$. Equation (7) is similar to (1) and in the absence of the buoyancy term it is identical; the nonlinear drift $\mathbf{v}(t)$ is defined by the second term and the nonlinear (capillary) dispersion coefficient by the third term on the right of (7).

[14] Here, we want to focus on problems where viscous forces dominate the flow and as such we neglect the influence of buoyancy and capillary pressure. This problem of immiscible two phase viscous dominated flow is commonly known as the Buckley-Leverett problem. With these approximations, the governing equation (7) reduces to the Buckley-Leverett equation

$$\frac{\partial S(\mathbf{x},t)}{\partial t} + \frac{\mathrm{d}\psi(S)}{\mathrm{d}S} q(\mathbf{x},t) \cdot \nabla S(\mathbf{x},t) = 0. \tag{9}$$

[15] In this work we consider the commonly studied problem of one fluid displacing another immiscible one. As was done by *Neuweiler et al.* [2003], we focus on fluid movement in a horizontal two-dimensional porous medium which is initially filled with fluid 2. Such a scenario eliminates buoyancy effects. We focus on neutrally stable displacement cases. Fluid 1 is injected along a line at a fixed rate, displacing fluid 2. We consider flow far away from the domain boundaries and thus disregard boundary effects. The resulting mean pressure gradient is then aligned with the one direction of the coordinate system. The corresponding homogeneous multiphase flow problem is $d = 1$ dimensional.

2.2. Homogeneous Solution

[16] Before studying the heterogeneous problem we briefly summarize the classical homogeneous case here. We denote the homogeneous solution as S_0 as this corresponds to the zeroth-order perturbation solution outlined in Appendix A. The governing equation is given by

$$\frac{\partial S_0(\mathbf{x},t)}{\partial t} + q(t) \frac{\mathrm{d}\psi(S_0)}{\mathrm{d}S_0} \frac{\partial S_0(\mathbf{x},t)}{\partial x_1} = 0. \tag{10}$$

The solution of this problem is discussed extensively in many textbooks [e.g., *Marle*, 1981]. Because of the hyperbolic nature of (10) the displacing fluid develops a shock front. Using the method of characteristics and the shock condition, one derives for $S_0(\mathbf{x}, t)$

$$S_0(x_1,t) = S^r\left[\frac{x_1}{x_f(t)}\right] H\left[x_f(t) - x_1\right], \tag{11}$$

where $H(x)$ is the heaviside step function [*Abramowitz and Stegun*, 1970] and the front position $x_f(t)$ is obtained from mass balance considerations as

$$x_f(t) = \frac{\mathrm{d}\psi(S^f)}{\mathrm{d}S^f} \int_0^t \mathrm{d}t' q(t'), \tag{12}$$

with S^f the front saturation. The latter is determined by the Welge tangent method [e.g., *Marle*, 1981]. The rear saturation $S^r[x_1/x_f(t)]$ behind the shock front is obtained by the method of characteristics. Note that $S_0(\mathbf{x}, t) = S_0(x_1, t)$ depends only on the one direction. A sample set of solutions for (10) are shown in Figure 1. Note that the fractional flow function is given by

$$\psi(S_0) = \psi(S^r) H\left[x_f(t) - x_1\right]. \tag{13}$$

2.3. Stochastic Model

[17] We employ a stochastic modeling approach in order to quantify the impact of medium heterogeneity and temporal pressure fluctuations on the saturation front of the displacing fluid. The spatial variability of the intrinsic permeability $k(\mathbf{x})$ and temporal variability of the injection rate are each modeled as stationary correlated stochastic processes in space and time, respectively. The two processes are not correlated. Permeability is characterized in terms of its logarithm, the log permeability $f(\mathbf{x}) = \ln k(\mathbf{x})$. The mean value of the latter is constant $\overline{f(\mathbf{x})} = \overline{f}$, where the average over all typical realizations of $k(\mathbf{x})$ is denoted by the overbar. The fluctuations of $f(\mathbf{x})$ about its mean value are defined by $f'(\mathbf{x}) = f(\mathbf{x}) - \overline{f}$. Its correlation function is defined by

$$\overline{f'(\mathbf{x}) f'(\mathbf{x}')} \equiv \sigma_{ff}^2 C_{ff}(\mathbf{x} - \mathbf{x}'). \tag{14}$$

[18] Temporal fluctuations are introduced via temporal variations in the boundary flux of the displacing fluid(see the discussion in Appendix B). The temporal variability of the boundary flux is modeled as a stationary correlated temporal random process $\mathbf{q}(t)$ whose mean $\langle \mathbf{q}(t) \rangle = q\mathbf{e}_1$ is aligned with the one direction of the coordinate system. The angular brackets in the following denote the ensemble average over all realization of the process $\mathbf{q}(t)$.

[19] In the following, we consider injection of the displacing fluid at an injection plane perpendicular to the one direction of the coordinate system and thus we assume the boundary flux to be aligned with $\mathbf{e}_1$, $\mathbf{q}(t) = q(t)\ \mathbf{e}_1$. The fluctuations of $q(t)$ about its mean value are defined by, $q'(t) = q(t) - q$. They are characterized by the correlation function

$$\langle q'(t) q'(t') \rangle = q^2 \sigma_t^2 C_t(t - t'). \tag{15}$$

[20] The spatiotemporal randomness is mapped onto the phase discharges and thus on the total discharge via the Darcy equation (2), which renders the total discharge a spatiotemporal random field. The latter can be decomposed according to (see Appendix B)

$$\mathbf{q}(\mathbf{x},t) = \mathbf{q}(t)\mathbf{e}_1 + \mathbf{q}'(\mathbf{x},t), \tag{16}$$

where $\mathbf{q}'(\mathbf{x}, t)$ is approximately given by (see Appendix B)

$$q_i'(\mathbf{x},t) = \mathbf{q}(t) \int \frac{\mathrm{d}k^{\mathbf{d}}}{(2\pi)^d} \exp(-\mathrm{i}\mathbf{k} \cdot \mathbf{x}) p_i(k) \tilde{f}'(\mathbf{k}), \tag{17}$$

with $\tilde{f}'(\mathbf{k})$ the Fourier transform of the log permeability fluctuation $f'(\mathbf{x})$; the $p_i(\mathbf{k})$ are defined by $p_i(\mathbf{k}) = \delta_{i1} - k_i k_1/\mathbf{k}^2$. Note that (17) is identical to the solution for single phase flow. This approximation is justified as long as the principal direction of the variation of saturation can be assumed to be aligned with the direction of $\mathbf{q}(\mathbf{x}, t)$.

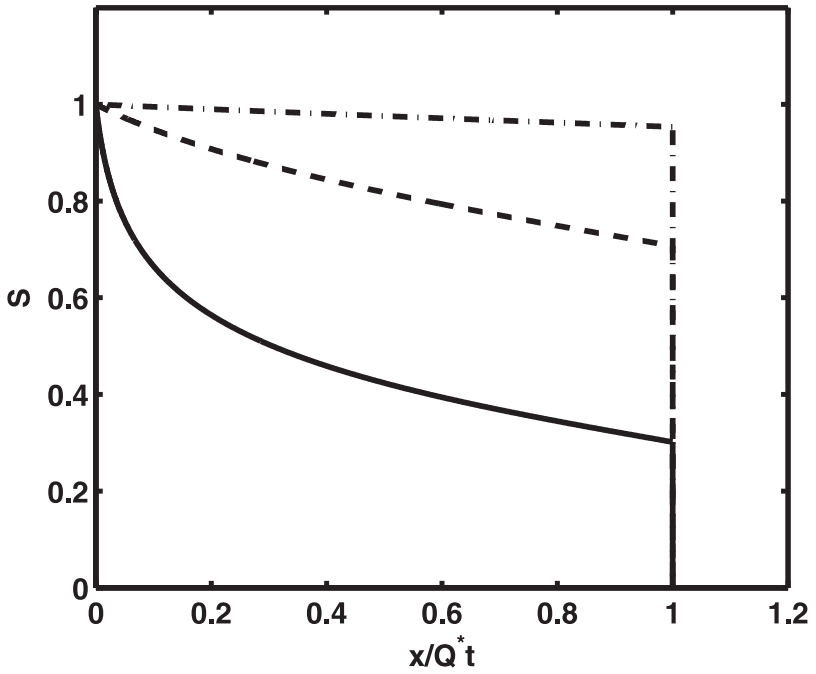

Figure 1. Solutions to the Buckley-Leverett problem for three different mobilities, assuming quadratic relative permeability saturation relationships (i.e., $k_{r1} = S^2$ and $k_{r2} = (1 - S)^2$). The curves show three different viscosity ratios (mobilities), $\mu = \mu_1/\mu_2$, namely, $\mu = 0.1$ (solid line), $\mu = 1$ (dashed line), and $\mu = 10$ (dash-dotted line). As the mobility increases, the flow approaches ideal displacement.

[21] Thus, we obtain for the velocity correlation

$$\overline{q_i'(\mathbf{x},t)q_j'(\mathbf{x}',t')} \equiv \sigma_{ff}^2 C_{ij}(\mathbf{x}-\mathbf{x}')q(t)q(t'), \tag{18}$$

where we defined

$$C_{ij}(\mathbf{x}) = \int \frac{\mathrm{d}k^d}{(2\pi)^d} \exp(-\mathrm{i}\mathbf{k}\cdot\mathbf{x}) p_i(\mathbf{k}) p_j(\mathbf{k}) \tilde{C}_{ff}(\mathbf{k}), \tag{19}$$

where $\tilde{C}_{ff}(\mathbf{k})$ is the Fourier transform of the log conductivity fluctuations.

[22] Here we have found specific conditions under which we approximate the covariance of the velocity field as the covariance of a single phase flow field. However, one must be cautious in doing this as this may not be correct for the unstable or stabilizing cases. In the unstable case viscous fingering dominates while for the stabilizing case the velocity field is no longer stationary as the velocity variance in the vicinity of the front is suppressed [e.g., *Noetinger et al.*, 2004].

3. Large-Scale Flow Behavior

[23] In the following, we derive large-scale flow equations by averaging the original local-scale flow equation. We define measures for the front spreading due to spatiotemporal fluctuations and for the front uncertainty due to temporal fluctuations. On the basis of these considerations we suggest a large-scale effective flow equation for the average saturation.

3.1. Average Flow Equation

[24] In analogy to solute transport in heterogeneous media [e.g., *Gelhar and Axness*, 1983; *Koch and Brady*, 1987; *Neuman*, 1993; *Cushman et al.*, 1994], here the spread of the space average saturation front $\overline{S}(\mathbf{x},t)$ due to spatial heterogeneity is modeled by a non-Markovian effective equation. Note that an effective equation is in general non-Markovian [e.g., *Zwanzig*, 1961; *Kubo et al.*, 1991; *Koch and Brady*, 1987; *Cushman et al.*, 1994; *Neuman*, 1993], which is expressed by spatiotemporal nonlocal flux terms. Under certain conditions, these fluxes can be localized.

[25] We follow the methodology routinely applied when deriving average dynamics [e.g., *Koch and Brady*, 1987; *Neuman*, 1993; *Cushman et al.*, 1994; *Tartakovsky and Neuman*, 1998a], which consists of (1) separating the saturation into mean and fluctuating components, (2) establishing a (nonclosed) system of equations for the average saturation and the saturation fluctuations, and (3) closing the system by disregarding terms that are of higher order in the fluctuations. It is known that perturbative solutions of advective-dispersion equations can sometimes result in bimodal behavior of averaged concentration fields [*Jarman and Russell*, 2003; *Morales-Casique et al.*, 2006; *Jarman and Tartakovsky*, 2008]. However, herein we do not encounter such concerns.

[26] Substituting (16) into (19) the local-scale equation for the saturation $S(\mathbf{x}, t)$ is given by

$$\frac{\partial S(\mathbf{x},t)}{\partial t} + \mathbf{q}(t)\cdot\nabla\psi(S) + \mathbf{q}'(\mathbf{x},t)\cdot\nabla\psi(S) = 0. \tag{20}$$

[27] In analogy to the decomposition of total discharge and permeability, we assume that the saturation can be decomposed into its spatial ensemble average $\overline{S}(\mathbf{x},t) \equiv \overline{S}(\mathbf{x},t)$ and fluctuations about it:

$$S(\mathbf{x},t) = \overline{S}(\mathbf{x},t) + S'(\mathbf{x},t). \tag{21}$$

[28] Furthermore assuming that the saturation fluctuations are small, we can expand the fractional flow function about the mean saturation according to

$$\psi(S) = \psi(\overline{S}) + \frac{\mathrm{d}\psi(\overline{S})}{\mathrm{d}\overline{S}} S'(\mathbf{x},t) + \ldots. \tag{22}$$

We take this expansion to $O(S')$ only as it has been shown that higher-order terms play an unimportant role [*Efendiev and Durolfsky*, 2002; *Neuweiler et al.*, 2003].

[29] Inserting (21) and (22) into (20), we obtain

$$\frac{\partial \overline{S}(\mathbf{x},t)}{\partial t} + \frac{\partial S'(\mathbf{x},t)}{\partial t} + \mathbf{q}(t)\cdot\nabla\psi(\overline{S}) + \mathbf{q}(t)\cdot\nabla\frac{\mathrm{d}\psi(\overline{S})}{\mathrm{d}\overline{S}} S'(\mathbf{x},t) + \mathbf{q}'(\mathbf{x},t)\cdot\nabla\psi(\overline{S}) = -\mathbf{q}'(\mathbf{x},t)\cdot\nabla\frac{\mathrm{d}\psi(\overline{S})}{\mathrm{d}\overline{S}} S'(\mathbf{x},t). \tag{23}$$

[30] Averaging the latter over the spatial ensemble gives

$$\frac{\partial \overline{S}(\mathbf{x},t)}{\partial t} + q(t)\cdot\nabla\psi(\overline{S}) = -\nabla\cdot\overline{\mathbf{q}'(\mathbf{x},t)S'(\mathbf{x},t)}\frac{\mathrm{d}\psi(\overline{S})}{\mathrm{d}\overline{S}}. \tag{24}$$

Subtracting (24) from (23), we obtain an equation for the saturation fluctuations

$$\frac{\partial S'(\mathbf{x},t)}{\partial t} + q(t)\cdot\nabla\frac{\mathrm{d}\psi(\overline{S})}{\mathrm{d}\overline{S}} S'(\mathbf{x},t) = -\mathbf{q}'(\mathbf{x},t)\cdot\nabla\psi(\overline{S}) - q'(\mathbf{x},t)\cdot\nabla\frac{\mathrm{d}\psi(\overline{S})}{\mathrm{d}\overline{S}} S'(\mathbf{x},t) + \nabla\cdot\overline{\mathbf{q}'(\mathbf{x},t)S'(\mathbf{x},t)}\frac{\mathrm{d}\psi(\overline{S})}{\mathrm{d}\overline{S}}. \tag{25}$$

This system of equations is not closed with respect to the average saturation. Our closure approximation consists in disregarding terms which are quadratic in the fluctuations in (25). Thus (25) reduces to

$$\frac{\partial S'(\mathbf{x},t)}{\partial t} + \mathbf{q}(t)\cdot\nabla\frac{\mathrm{d}\psi(\overline{S})}{\mathrm{d}\overline{S}} S'(\mathbf{x},t) = -\mathbf{q}'(\mathbf{x},t)\cdot\nabla\psi(\overline{S}). \tag{26}$$

This is then solved with the associated Green function, i.e.,

$$S'(\mathbf{x},t) = -\int_0^t \int d^d\mathbf{x}' G(\mathbf{x},t|\mathbf{x}',t')\mathbf{q}'(\mathbf{x}',t')\cdot\nabla'\psi\left[\overline{S}(\mathbf{x}',t')\right], \tag{27}$$

where $G(\mathbf{x}, t|\mathbf{x}', t')$ solves

$$\frac{\partial G(\mathbf{x},t|\mathbf{x}',t')}{\partial t} + \mathbf{q}(t)\cdot\nabla\frac{\mathrm{d}\psi(\overline{S})}{\mathrm{d}\overline{S}} G'(\mathbf{x},t|\mathbf{x}',t') = 0 \tag{28}$$

for the initial condition $G(\mathbf{x}, t|\mathbf{x}', t') = \delta(\mathbf{x} - \mathbf{x}')$. Inserting (26) into (24), we obtain a nonlinear upscaled equation for the (space) average saturation

$$\frac{\partial \overline{S}(\mathbf{x},t)}{\partial t} + \mathbf{q}(t)\cdot\frac{\mathrm{d}\psi(\overline{S})}{\mathrm{d}\overline{S}(\mathbf{x},t)}\nabla\overline{S}(\mathbf{x},t) - \nabla\cdot\int_0^t \mathrm{d}t' \int d^dx' \left[\frac{\mathrm{d}\psi(\overline{S})}{\mathrm{d}\overline{S}(\mathbf{x},t)} k(\mathbf{x},t|\mathbf{x}',t') \frac{\mathrm{d}\psi(\overline{S})}{\mathrm{d}\overline{S}(\mathbf{x}',t')}\right]\nabla'\overline{S}(\mathbf{x}',t') = 0, \tag{29}$$

where we define the kernel

$$k_{ij}(\mathbf{x},t|\mathbf{x}',t') = \overline{q_i'(\mathbf{x},t)G(\mathbf{x},t|\mathbf{x}',t')q_j'(\mathbf{x}',t')}. \tag{30}$$

[31] Equation (29) has a similar structure as (1), but is characterized by a spatiotemporal nonlocal dispersive flux. As outlined above, such nonlocal fluxes typically occur when averaging. Note that the nonlinear character of the two-phase problem is preserved during the upscaling exercise. The nonlinearity of the problem is quasi-decoupled in terms of the Green function; equation (28) for $G(\mathbf{x}, t|\mathbf{x}', t')$ is linear but depends on the average saturation. Appendix C provides explicit perturbation theory expressions for the Green function.

3.2. The Kernel

[32] Approximating the Green function $G(\mathbf{x}, t|\mathbf{x}', t')$ by (C4), where we assume that the average saturation is reasonably represented by the homogeneous zeroth-order saturation S_0 according to

$$G(\mathbf{x},t|\mathbf{x}',t') = G_0(x_1,t|x_1',t')\delta(\mathbf{y}-\mathbf{y}'). \tag{31}$$

The kernel, defined in (30), becomes

$$k_{ij}(\mathbf{x},t|\mathbf{x}',t') = k_{ij}(x_1,t|x_1',t')\delta(\mathbf{y}-\mathbf{y}'), \tag{32}$$

where $k_{ij}(x_1, t|x'_1, t')$ is defined by

$$k_{ij}(x_1,t|x_1',t') = \sigma_{ff}^2 C_{ij}(x_1 - x_1')q(t)q(t')\frac{1}{x_1(t)}\delta\left[\frac{x_1'}{x_1(t')} - \frac{x_1}{x_1(t)}\right]. \tag{33}$$

Here we set $C_{ij}(x_1, t, t') \equiv C_{ij}(\mathbf{x}, t, t')|_{\mathbf{y}=\mathbf{0}}$ and $x_1(t) = \int_0^t \mathrm{d}t' q(t')$. In the following section, we determine effective measures for the spread of the front saturation depending on the kernel $k_{ij}(x_1, t|x'_1, t')$. Contributions in transverse directions vanish, because of the particular displacement scenario under consideration [see also *Neuweiler et al.*, 2003]. Thus, we focus our attention on the spread of the saturation in one direction.

3.3. Saturation Dispersion

[33] We quantify the front spreading in single realizations of the temporal random process in terms of spatial moments and then perform the ensemble average over the resulting observables. This procedure quantifies the combined effect of spatial and temporal fluctuations on the spread of the saturation front. Later we quantify the uncertainty of the front position due to purely temporal fluctuations. Appendix F illustrates the definitions of macrodispersion presented by *Neuweiler et al.* [2003] and *Langlo and Espedal* [1995] in terms of our developments here.

3.3.1. Spatial Moment Equations

[34] The objective here is to quantify the impact of heterogeneity and temporal fluctuations on the spread of the saturation front. In analogy to transport in single phase flow and given the similarity of the large-scale flow equation (29) with the advection-dispersion equation it is tempting to quantify the spread of the saturation distribution in terms of its spatial moments. However, the displacement of one fluid by another corresponds to a continuous injec-

tion in the analog case of solute transport in single phase flow. In the latter case, the spreading of the solute front cannot be quantified satisfactorily by the moments of the concentration distribution, but rather by the moments of its derivative in flow direction. Thus, here, instead of considering moments of saturation, we consider the moments of the derivative of the saturation in the i direction:

$$\bar{s}_i(\mathbf{x},t) = -A^{-1}\frac{\partial \overline{S}(\mathbf{x},t)}{\partial x_i}, \tag{34}$$

where A is the area of the injection plane located at $x_1 = 0$. This is motivated by the fact that the homogeneous solution develops a shock front, which is captured sharply by a derivative. We now normalize $s_1(\mathbf{x}, t)$ to 1:

$$\int_{x_1>0} \mathrm{d}^d x \bar{s}_1(\mathbf{x},t) = 1. \tag{35}$$

[35] The first and second moments of $s_1(\mathbf{x}, t)$ in the one direction are given by

$$m_1^{(1)} = \int \mathrm{d}^d x x_i s_1(\mathbf{x},t) \quad \text{and} \quad m_{11}^{(2)} = \int \mathrm{d}^{\mathbf{d}} x x_i^2 s_1(\mathbf{x},t). \tag{36}$$

With these we can calculate the second centered moment, $\kappa_{11} = m_{11}^{(2)} - m_1^{(1)}m_1^{(1)}$, which we can use to define an effective longitudinal dispersion coefficient. The equation governing the evolution of κ_{11} is derived in Appendix D and is given by

$$\begin{aligned}\frac{\partial \kappa_{11}(t)}{\partial t} = q(t)&\left[2A^{-1}\int \mathrm{d}^d x \psi\left[\overline{S}(\mathbf{x},t)\right] - \int_0^t \mathrm{d}t' q(t')\right] \\ &- 2A^{-1}\int \mathrm{d}^d x \int_0^t \mathrm{d}t' \int \mathrm{d}^d x' \frac{\mathrm{d}\psi(\overline{S})}{\mathrm{d}\overline{S}(\mathbf{x},t)} k_{1j}(\mathbf{x},t|\mathbf{x}',t') \\ &\cdot \frac{\partial}{\partial x_j'}\psi\left[\overline{S}(\mathbf{x}',t')\right].\end{aligned} \tag{37}$$

We identify the second term as the one that measures the actual spread of the saturation front due to spatial heterogeneity. In the absence of heterogeneity, the width of the saturation distribution behind the shock front is quantified by the first term on the right side. In that case, it quantifies a purely advective widening due to different flow velocities at the front and behind the front (see Appendix G). It grows in leading order with the square of time. Nevertheless, the saturation dispersion at the front acts (nonlinearly) on the width of the saturation distribution behind the disperse front.

3.3.2. Front Dispersion

[36] We now define the longitudinal macrodispersion coefficient $d_{ii}^s(t)$ in terms of the second term on the right side of (37) by

$$\begin{aligned}d_{11}^s(t) = -A^{-1}&\int \mathrm{d}^d x \int_0^t \mathrm{d}t' \int \mathrm{d}^d x' \frac{\mathrm{d}\psi(\overline{S})}{\mathrm{d}\overline{S}(\mathbf{x},t)} k_{1j}(\mathbf{x},t|\mathbf{x}',t') \\ &\frac{\partial}{\partial x_j'}\psi\left[\overline{S}(\mathbf{x}',t')\right].\end{aligned} \tag{38}$$

In order to evaluate (38), we approximate the average saturation by $\overline{S} = S_0(x_1, t)$, and substitute the kernel (32) to obtain

$$\begin{aligned}d_{11}^s(t) = -\sigma_{ff}^2 \int \mathrm{d}x_1 \int_0^t \mathrm{d}t' \int_0^\infty \mathrm{d}x_1' \frac{x_1}{x_1(t)} C_{11}(x_1 - x_1') q(t) q(t') \\ \times \frac{1}{x_1(t)}\delta\left[\frac{x_1'}{x_1(t')} - \frac{x_1}{x_1(t)}\right]\frac{\partial}{\partial x_1'}\psi\left\{S_0\left[\frac{x_1'}{x_f(t')}\right]\right\},\end{aligned} \tag{39}$$

where we used expression (C1) for $\mathrm{d}\psi(S_0)/\mathrm{d}S_0$.

[37] As outlined in Appendix E this can be simplified to

$$d_{11}^s(t) = \sigma_{ff}^2 q(t)\int_0^{qt} \mathrm{d}x_1 C_{11}(x_1) + \sigma_{ff}^2 \int_0^t \mathrm{d}t' q'(t') q(t) C_{11}(qt). \tag{40}$$

On average this gives

$$\left\langle d_{11}^s(t)\right\rangle = \sigma_{ff}^2 q \int_0^{qt} \mathrm{d}x_1 C_{11}(x_1) + \sigma_{ff}^2 \sigma_t^2 q^2 C_{11}(qt) \int_0^t \mathrm{d}t' C_t(t'). \tag{41}$$

The contribution due to temporal fluctuations decays to zero with increasing time as $C_{11}(qt)$ tends to zero for times larger than $\tau_u = l/q$. Thus, there is no significant contribution to front spreading due to temporal fluctuations. This is different from solute transport in single phase flow. In this case, there is a persistent macroscopic dispersion effect due to the interaction of spatial heterogeneity, temporal fluctuations [*Dentz and Carrera*, 2003] and local dispersion. The latter is the crucial (irreversible) mechanism, which activates heterogeneity and temporal fluctuations as a macroscopic spreading effect. Here, such irreversibility is lacking. The multiphase flow problem is fully reversible. Thus, temporal fluctuations play only a minor role for front spreading. In the presence of capillary dispersion as expressed by the nonlinear dispersive flux in (7), this may be different. However, this must be investigated in more detail as the influence of such a nonlinear dispersive flux is not obvious.

[38] The uncertainty associated with the front location due to temporal pressure fluctuations can be quantified in terms of the moments defined above as

$$\sigma_m^2(t) = \left\langle \left[m_1(t) - \left\langle m_1^{(1)}(t)\right\rangle\right]^2\right\rangle. \tag{42}$$

Inserting (D3) into (42), we obtain

$$\sigma_m^2(t) = q^2\sigma_t^2 \int_0^t \mathrm{d}t' \int_0^t \mathrm{d}t'' C_t(t' - t''). \tag{43}$$

Thus, the front uncertainty grows linearly with time for short-range temporal correlation of the pressure fluctuations. Note that the temporal center of mass fluctuations give rise to an artificial (ensemble) dispersion effect, which occurs for the saturation distribution averaged over the

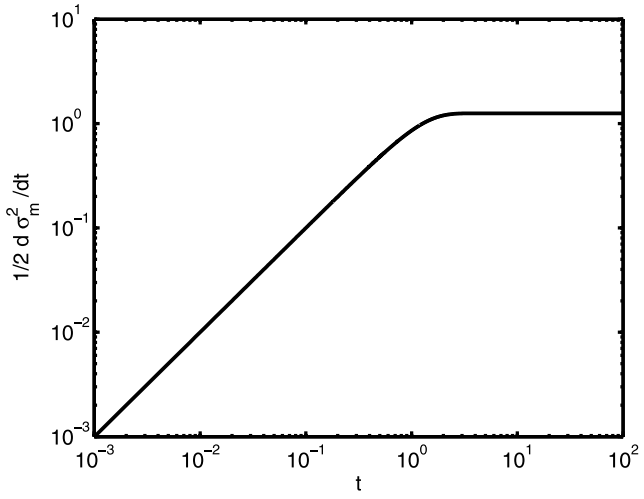

Figure 2. Evolution of the front uncertainty due to temporal fluctuations ($\frac{1}{2}\frac{d\sigma_m^2(t)}{dt}$), where ${\sigma_m}^2(t)$ is defined in (43)) for a Gaussian correlated field of correlation time 1 and variance 1.

temporal ensemble. A measure for this ensemble dispersion effect is the temporal derivative of (43), i.e., $\frac{1}{2}\frac{d\sigma_m^2(t)}{dt}$. A sample plot of this quantity for a Gaussian correlated temporal field with variance 1 and correlation time 1 is shown in Figure 2. At early times we see a growth, which at late times asymptotes to a constant value, corresponding to the late time linear growth in the variance.

[39] It is important to note that this ensemble dispersion is an artificial effect due to sample to sample fluctuations of the plume position from realization to realization. In a homogeneous medium the temporal fluctuations for various realizations results in a Buckley-Leverett front at different locations within each realization. The process of averaging over these realizations appears to smear out the sharp front and look like a dispersive effect. In reality however the sharp front exists for each of these cases and the averaging artificially masks it. For more details see the analysis in Appendix G. This effect is illustrated in Figure 3. In essence this term gives a measure of the uncertainty of the location of the front.

[40] Fluids with lower mobility ratios intrude faster as discussed in section 2.3.1. Therefore, the overall uncertainty associated with the front location can be particularly large

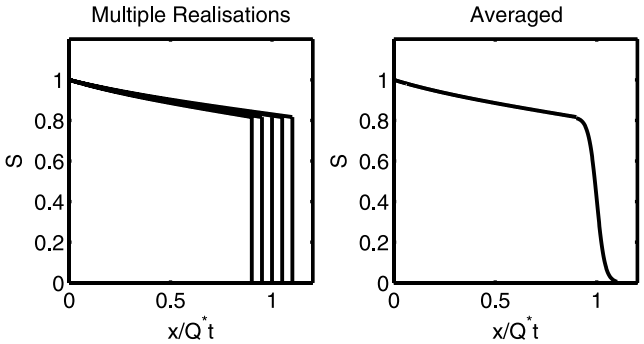

Figure 3. Illustration of the front uncertainty due to temporal fluctuations. This can be interpreted as an (artificial) ensemble dispersion effect.

Table 1. Inputs for Numerical Simulations

Case	σ_t^2	σ_k^2	Viscosity Ratio M	Medium	Temporal
a	0	0.5	0.5	Gaussian	none
b	0	1	0.5	Gaussian	none
c	0	0.5	0.5	Delta	none
d	0	1	0.5	Delta	none
e	0.5	0.5	0.5	Gaussian	sinusoidal
f	1	1	0.5	Gaussian	sinusoidal
g	0.25	0.5	0.5	Gaussian	Gaussian
h	0.5	1	0.5	Gaussian	Gaussian
i	0	0.5	0.2	Gaussian	none
k	0	0.5	0.2	Gaussian	sinusoidal
l	0.5	1	0.2	Gaussian	Gaussian

for small mobility ratios, which are often relevant in the field of CO_2 sequestration.

4. Numerical Simulations

[41] In order to test the models presented herein we also conducted a numerical study of the Buckley-Leverett problem in a heterogeneous medium. To do this we used an in-house finite volume code, which uses an implicit in pressure and explicit in saturation scheme [e.g., *Hasle et al.*, 2007]. The numerical dispersion using this method was found to be negligible compared with the effective dispersion we calculate.

[42] In all cases the domain size is 25 m $\times$ 8 m with a correlation length of 0.5 m. The mean permeability is 4.2×10^{-12} m s^{-1} with an average injection flow rate of 5×10^{-6} m s^{-1}. This values are identical to those from *Neuweiler et al.* [2003]. The numerical grid size is uniform with length 0.025 m, which means that we have 20 lengths within one correlation length. This grid is 4 times finer than *Neuweiler et al.* [2003] and was chosen after an extensive grid sensitivity study, which showed that the numerical solution was no longer sensitive to grid size. In total we consider eleven problems outlined in Table 1. Cases a–h are neutrally stable, while i–l are unstable.

[43] For each of these eleven cases numerical solutions with a minimum of 100 realizations of permeability fields

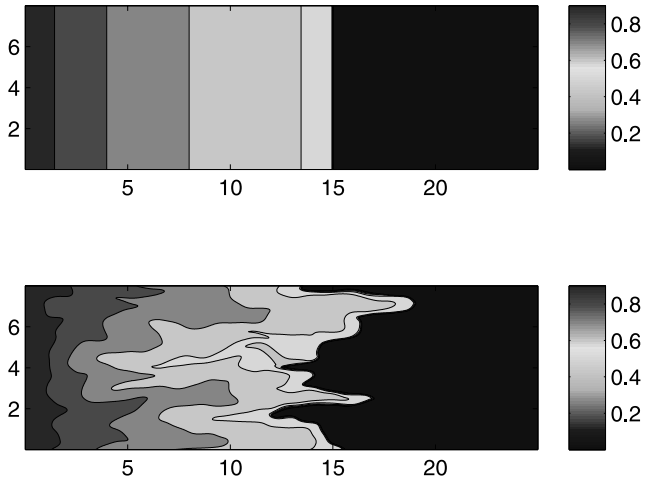

Figure 4. A sample image from the numerical simulations for case a for (top) a homogeneous field and (bottom) a heterogeneous field.

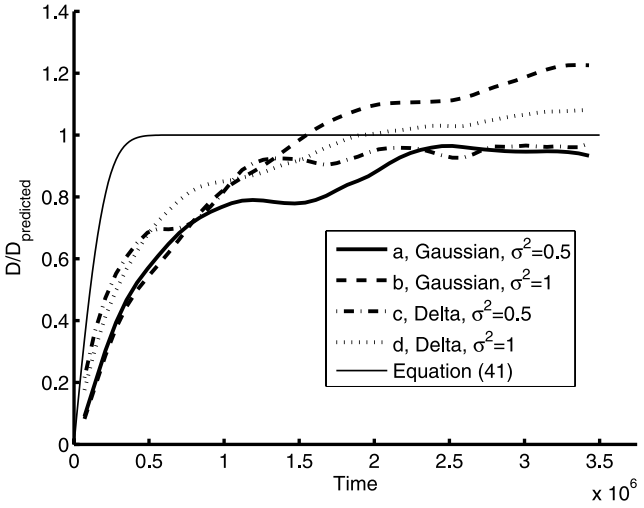

Figure 5. Numerically calculated dispersion coefficient normalized with the values predicted by (41) for cases a (solid line), b (dashed line), c (dash-dotted line), and d (dotted line). The thin solid line represents the time-dependent dispersion coefficient predicted by (41).

were conducted. The effective dispersion coefficient was then calculated using (D3), (D4) and (38).

[44] A sample contour of the saturation field for a homogeneous medium, which is equivalent to the homogeneous analytical solution in (11) is shown in Figure 4. Also, a contour corresponding to a heterogeneous medium case b is shown. We include Figure 4 to illustrate the spreading of the front that is induced by the heterogeneities.

[45] Figure 5 illustrates the time evolution of the dispersion coefficients calculated from cases a–d (normalized by the asymptotic value predicted by (41)). In all four cases the asymptotic value is well predicted with a slight overprediction for cases b and d. This is likely because $\sigma_{ff}^2 = 1$ is becoming large and the perturbative approach is no longer valid.

[46] In Figure 6 we plot the dispersion coefficient computed for case e. As case e is essentially case a with a temporally fluctuating flow rate we also include the dispersion coefficient corresponding to case a. As expected, the dispersion coefficient varies sinusoidally in time in response to the fluctuating flow. Overall though, there is no enhanced dispersion due to the temporal fluctuations as when time averaged the dispersion coefficient for case e is the same as that of case a.

[47] At late times, the perturbation theory expression predicts front spreading well up to variances of $\sigma_{ff}^2 = 1$. At early times, the perturbation expression predicts a much faster increase of the dispersion coefficient. We attribute this to boundary effects. This is because the perturbation solution to the two-phase flow problem is only valid at large distances from the boundaries. At early times, however, the front is still close to the injection boundary and thus, the perturbation solution (17) presents limited validity.

[48] The dispersion coefficient responds linearly to the flow speed never exceeding the dispersion coefficient associated with the maximum flow rate and never falling below that associated with the lower flow speed as indicated by the dotted lines. We do not include a figure illustrating case f, which is similar to case e, but with greater amplitude of fluctuation. This is because the behavior is identical, but with larger amplitude of fluctuation, and offers no new insight. Cases g and h display a similar behavior. However as the injection flow rate is random the dispersion coefficient varies in a more random manner reflecting this. The temporally averaged dispersion coefficient is still the same as that predicted in case a.

[49] The last three cases we consider, namely, i, k and l, are for a viscosity ratio $M = 0.2$, which is known to be affected by the Saffman Taylor instability [*Marle*, 1981; *Blunt et al.*, 1994]. It is also known that heterogeneity can

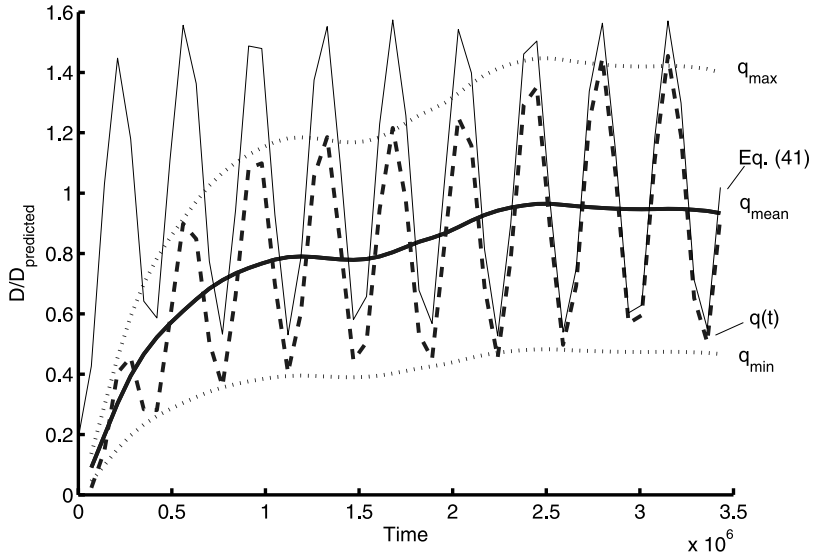

Figure 6. Numerically calculated dispersion coefficient normalized with the values predicted by (41) for cases a (solid line) and e (dashed line). The dotted lines represent the effective dispersion coefficient for case a at the maximum and minimum values of the flow rate associated with the sinusoid. The thin solid line represents the time-varying solution predicted with (41).

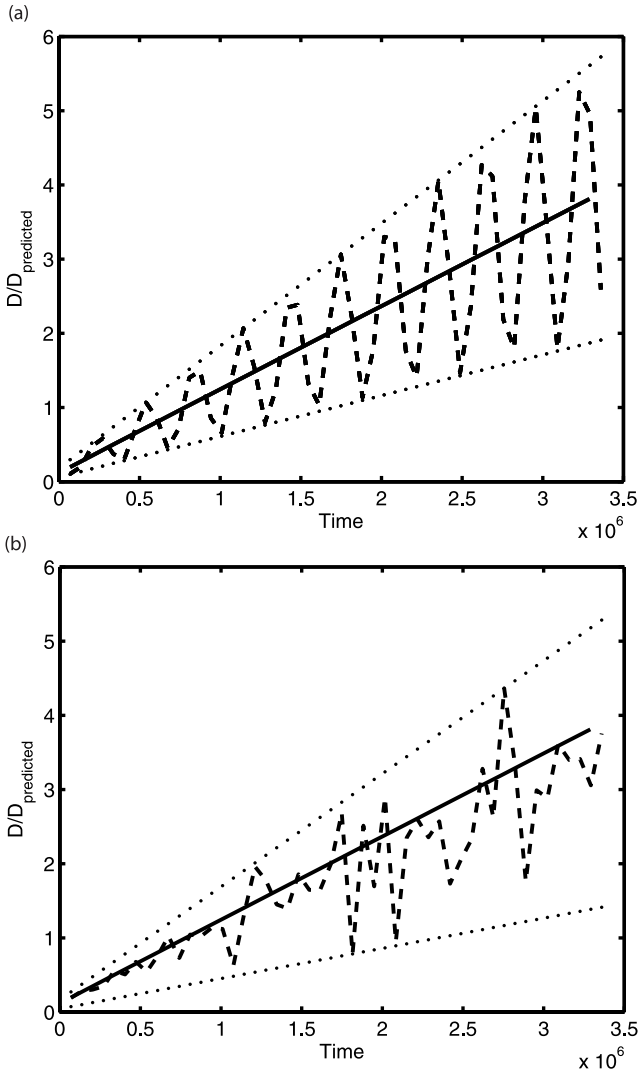

Figure 7. Numerically calculated dispersion coefficient normalized with the values predicted by (41) for (top) cases j (solid line) and k (dashed line) and (bottom) one temporal realization of case a (dashed line). The dotted lines represent the effective dispersion coefficient for case k at the maximum and minimum values of the flow rate associated with the temporal flow fields.

have a stabilizing or destabilizing effect depending on boundary conditions and the mobility ratio [*Tartakovsky et al.*, 2003]. While the focus of this work is not to look at unstable cases, one of the motivations of this study is to understand how medium heterogeneities and temporal fluctuations might influence injection of CO_2 during sequestration. Values of M for CO_2 and water vary between $\frac{1}{5}$ and $\frac{1}{50}$ (J. Garcia and K. Preuss, Flow instabilities during injection of CO_2 into saline aquifers, paper presented at TOUGH Symposium 2003, Lawrence Berkeley National Laboratory, Berkeley, California, 2003), which are all susceptible to this instability. Figure 7 illustrates the "dispersion" coefficient as calculated with our expression (41). Clearly our model fails to capture this behavior as we do not account for the possibility of this instability. Instead the dispersion coefficient grows linearly/ballistically suggesting advection drives the instability; a similar observation was made by Garcia and Preuss (presented paper, 2003) where the growth of the fingers associated with the instability grew almost linearly in time. As the focus of this work was to study the influence of temporal fluctuations in the flow it is worth noting that the same conclusions appear to hold for the unstable case as for the stable case. While the fluctuations do enhance and decrease the effective dispersion over time, on average there is no effect. Case l reveals a similar behavior.

5. Summary and Conclusions

[50] We investigated the idealized displacement of one fluid by another immiscible fluid in a heterogenous porous medium subjected to temporal fluctuations. We employed the Buckley-Leverett model to study the impact of spatiotemporal fluctuations on the effective two-phase flow behavior. By averaging the transport equation for saturation over the spatial ensemble, we derived a nonlinear effective equation for the average saturation, which is characterized by a spatiotemporally nonlocal dispersive flux term. This term quantifies the impact of spatial heterogeneity on the spreading of the saturation front. Using spatial moments of the gradient of saturation we derived an effective large-scale dispersion coefficient that quantifies the spreading of the saturation front.

[51] In contrast to the conservative solute case, we find that temporal fluctuations have a very minor impact on the dispersion of the saturation front. However, they can significantly increase the uncertainty of the front position, particularly when the viscosity of the fluid being injected is much smaller than that being displaced as is typically the case for geological carbon sequestration where the viscosity of CO_2 can be 5 to 80 times less than that of water (Garcia and Preuss, presented paper, 2003). For single phase flow, temporal fluctuations enhance spreading due to the irreversibility of local diffusion. Such a mechanism is lacking in the Buckley-Leverett model. Additionally, the current model neglects other effects such as microscale trapping [*Pop and Schweizer*, 2007], which can lead to irreversible behavior. Therefore, we conjecture that accounting for capillarity and other mechanisms, which appear to act in a "diffusive" manner, may potentially lead to an enhancement of spreading due to temporal flow fluctuations. On the basis of our analysis, we have proposed an effective flow description, which is based on (1) the effective nonlocal flow equation and (2) the measure of front uncertainty in terms of the fluctuations of the first moment of the saturation front.

[52] To complement our analytical model, we performed numerical simulations of the (Buckley-Leverett) two-phase flow problem in heterogeneous permeability fields. For log conductivities with variances of up to 1 the model seems to provide very satisfactory results, particularly at late times. At early times there is a discrepancy, which is when boundary effects can still play an important role.

[53] The analytical results presented here are only valid for neutrally stable displacement. However, in many cases of practical interest, particularly CO_2 sequestration, the mobility ratios are small leading to Saffman-Taylor instabilities [*Saffman and Taylor*, 1958; *Blunt et al.*, 1994], which can enhance spreading even further. Using the measures for spreading developed herein, we studied the dispersion of a saturation front in such unstable scenarios.

We find that the instabilities cause a ballistic growth of the width of the saturation front, which can be explained by the advective nature of this phenomenon. However, in similar fashion to the stable flow scenarios, the numerical simulations indicate that temporal fluctuations do not on average affect spreading in unstable flows either. Consequently, from a practical perspective, this suggests that there is little potential benefit to be gained by deliberate temporal hydraulic manipulation of the flow. For cases where capillarity plays an important role this may not be the case and further investigation is warranted. Additionally, further work that incorporates buoyancy should be conducted, as this can clearly play an important role in such flows.

Appendix A: Perturbation Theory

[54] Here we briefly summarize and generalize the perturbation theory for the saturation solution of the Buckley-Leverett problem as given by *Neuweiler et al.* [2003].

[55] We write the decomposition (16) of the total flow velocity as

$$\mathbf{q}(\mathbf{x},t) = \mathbf{q}(t)\mathbf{e}_1 + \epsilon\mathbf{q}'(\mathbf{x},t), \tag{A1}$$

where ϵ is a book keeping parameter that will be set to 1 later. We now assume that the saturation $S(\mathbf{x}, t)$ can be expanded into a series in powers of ϵ

$$S(\mathbf{x},t) = \sum_{i=0}^{\infty} \epsilon^i S_i(\mathbf{x},t). \tag{A2}$$

Substituting these expansions into the governing equation (10) and collecting orders of ϵ yields a hierarchy of linear equations for the $S_i(\mathbf{x}, t)$.

[56] At zeroth order, S_0 is identical to the homogeneous solution described in section 2.2. At first and second order in ϵ we obtain for $S_1(\mathbf{x}, t)$

$$\frac{\partial S_1(\mathbf{x},t)}{\partial t} + Q\nabla\left(\frac{\mathrm{d}\psi(S_0)}{\mathrm{d}S_0}S_1(\mathbf{x},t)\right) = -q'(\mathbf{x},t)\nabla\psi_0(S_0), \tag{A3}$$

and for $S_2(\mathbf{x}, t)$

$$\frac{\partial S_2(\mathbf{x},t)}{\partial t} + Q\nabla\left(\frac{\mathrm{d}\psi(S_0)}{\mathrm{d}S_0}S_2(\mathbf{x},t) + \frac{1}{2}\frac{\mathrm{d}^2\psi S_0}{\mathrm{d}S_0^2}|S_1(\mathbf{x},t)^2\right) = -q'(\mathbf{x},t)\nabla\left(\frac{\mathrm{d}\psi_0}{\mathrm{d}S_0}S_1(\mathbf{x},t)\right). \tag{A4}$$

At each approximation order, the equations are linear and can be solved by using the associated Green function, which gives for $S_1(\mathbf{x}, t)$

$$S_1(\mathbf{x},t) = -\int_{\mathbf{0}}^{t}\mathrm{d}t'\int \mathrm{d}x_1' G_0(x_1,t|x_1',t')q_1'(x_1',\mathbf{y},t') \cdot\frac{\partial}{\partial x_1'}\psi[S_0(x_1',t')], \tag{A5}$$

where $\mathbf{y} = (x_2, \ldots, x_d)^T$. The Green function $G_0(x_1, t|x'_1, t')$ solves

$$\frac{\partial G_0(x_1,t|x_1',t')}{\partial t} + q(t)\frac{\mathrm{d}\psi(S_0)}{\mathrm{d}S_0}\frac{\partial G_0(x_1,t|x_1',t')}{\partial x_1} = 0 \tag{A6}$$

for the initial condition $G_0(x_1, t'|x'_1, t') = \delta(x_1 - x'_1)$. Appendix C gives a solution for $G_0(x_1, t|x'_1, t')$ for arbitrary $q(t)$.

Appendix B: Correlations

[57] The Buckley-Leverett formulation assumes that capillary pressure $p_c = p_1 - p_2$ is constant, p_c = constant, and disregards buoyancy effects. Then, the Darcy system (2) reduces to

$$\mathbf{q}^{(i)}(\mathbf{x},t) = -\frac{k(\mathbf{x})k_{ri}(S_i)}{\mu_i}\nabla p_1(\mathbf{x},t). \tag{B1}$$

[58] We obtain for the total flow velocity $\mathbf{q}(\mathbf{x}, t) = \mathbf{q}^{(1)}(\mathbf{x}, t) + \mathbf{q}^{(2)}(\mathbf{x}, t)$

$$\mathbf{q}(\mathbf{x},t) = -k(\mathbf{x})\Lambda(S)\nabla p_1(\mathbf{x},t), \tag{B2}$$

where we defined $\Lambda = \lambda_1(S) + \lambda_2(S)$.

[59] We consider here a flux boundary condition and specify the flux at the inflow boundary as

$$\mathbf{q}(\mathbf{x},t)|_{x_1=0} = \mathbf{e}_1 q(t), \tag{B3}$$

with the temporally varying boundary flux $q(t)$. The total flux then can be conveniently expressed by the vector potential $\mathbf{A}(\mathbf{x}, t)$

$$\mathbf{q}(\mathbf{x},t) = \nabla\times\mathbf{A}(\mathbf{x},t). \tag{B4}$$

We have the freedom to choose an arbitrary value for the divergence of $\mathbf{A}(\mathbf{x}, t)$ because it is invariant under the gauge transformation $\hat{\mathbf{A}}(\mathbf{x}, t) = \mathbf{A}(\mathbf{x}, t) + \nabla\phi(\mathbf{x}, t)$, with a scalar function $\phi(\mathbf{x}, t)$. Here we choose the Coulomb gauge $\nabla\cdot\mathbf{A}(\mathbf{x}, t) = 0$.

[60] Using these definitions in (B2) and taking the rotation of the resulting equation, we obtain

$$\Delta\mathbf{A}(\mathbf{x},t) + \nabla f(\mathbf{x})\times\mathbf{q}(\mathbf{x},t) + \nabla f^{\Lambda}(S)\times\mathbf{q}(\mathbf{x},t) = 0, \tag{B5}$$

where we defined

$$f(\mathbf{x}) = \ln k(\mathbf{x}), \qquad f^{\Lambda}(S) = \ln\Lambda(s). \tag{B6}$$

The log-hydraulic conductivity is divided into mean and fluctuations about it as outlined in section 2.3.

[61] The principal direction of the variation of saturation in the respective fluid will be aligned with the direction of $\mathbf{q}(\mathbf{x}, t)$ so that the cross product of the saturation gradient and total flow velocity is approximately zero

$$\nabla f^{\Lambda}(S)\times\mathbf{q}(\mathbf{x},t) = \frac{\mathrm{d}f^{\Lambda}(S)}{\mathrm{d}S}[\nabla S\times\mathbf{q}(\mathbf{x},t)] \approx 0, \tag{B7}$$

and we can approximate (B5) by

$$\Delta\mathbf{A}(\mathbf{x},t) + \nabla f(\mathbf{x})\times[\nabla\times\mathbf{A}(\mathbf{x},t)] \approx 0. \tag{B8}$$

[62] Because of mass conservation and statistical stationarity of the random permeability $k(\mathbf{x})$, the average flux

must be equal to the boundary flux and thus the rotation of $\mathbf{A}(\mathbf{x}, t)$ can be decomposed into

$$\nabla \times \mathbf{A}(\mathbf{x}, t) = \mathbf{e}_1 q(t) + \nabla \times \mathbf{A}'(\mathbf{x}, t). \tag{B9}$$

Inserting the latter into (B8), we obtain for $\mathbf{A}'(\mathbf{x}, t)$

$$\Delta \mathbf{A}'(\mathbf{x}, t) = -\nabla f'(\mathbf{x}) \times \mathbf{e}_1 q(t) - \nabla f'(\mathbf{x}) \times [\nabla \times \mathbf{A}'(\mathbf{x}, t)]. \tag{B10}$$

[63] Disregarding terms that are quadratic in the fluctuations and assuming flow far away from the injection boundary, the latter gives the well known first-order approximation for $\mathbf{q}'(\mathbf{x}, t)$ [e.g., *Gelhar and Axness*, 1983; *Rehfeldt and Gelhar*, 1992; *Dentz and Carrera*, 2005]

$$q_i'(\mathbf{x}, t) = q(t) \int \frac{\mathrm{d}^d k}{(2\pi)^d} \exp(-\mathrm{i}\mathbf{k} \cdot \mathbf{x}) \left(\delta_{i1} - \frac{k_1 k_i}{k^2} \right) \tilde{f}'(\mathbf{k}), \tag{B11}$$

where $\tilde{f}'(\mathbf{k})$ is the Fourier-transform of the log-hydraulic conductivity fluctuations.

Appendix C: Green Function

[64] Using the method of characteristics for the homogenous Buckley-Leverett problem, it can be shown that the derivative of the fractional flow function at $S_0(x_1, t)$ is given by

$$\frac{\mathrm{d}\psi_0}{\mathrm{d}S_0} = \frac{x_1}{x_1(t)}, \tag{C1}$$

where we defined

$$x_1(t) = \int_0^t \mathrm{d}\tau q(\tau). \tag{C2}$$

This yields for (A6)

$$\frac{\partial G_0(x_1, t|x_1', t')}{\partial t} + \frac{\mathrm{d}}{\mathrm{d}t} \ln[x_1(t)] \frac{\partial}{\partial x_1} x_1 G_0'(x_1, t|x_1', t') = 0. \tag{C3}$$

[65] Equation (C3) can be solved using the method of characteristics, which gives

$$G_0(x_1, t|x_1', t') = \frac{1}{x_1(t)} \delta \left[\frac{x_1}{x_1(t)} - \frac{x_1'}{x_1(t')} \right]. \tag{C4}$$

For constant spatial mean velocity, $q(t) = q$, the Green function is given by [e.g., *Neuweiler et al.*, 2003]

$$g_0(x_1, t|x_1', t') = \frac{1}{t} \delta \left(\frac{x_1}{t} - \frac{x_1'}{t'} \right). \tag{C5}$$

Appendix D: Moment Equations

[66] Taking the derivative of (29) with respect to x_i results in an equation for $s_i(\mathbf{x}, t)$

$$\frac{\partial \overline{s}_i(\mathbf{x}, t)}{\partial t} + \mathbf{q}(t) \cdot \frac{\partial}{\partial x_i} \frac{\mathrm{d}\psi(\overline{S})}{\mathrm{d}\overline{S}(\mathbf{x}, t)} \overline{\mathbf{s}}(\mathbf{x}, t) - \frac{\partial}{\partial x_i} \nabla \cdot \int_0^t \mathrm{d}t' \int \mathrm{d}^d x' \left[\frac{\mathrm{d}\psi(\overline{S})}{\mathrm{d}\overline{S}(\mathbf{x}, t)} \mathbf{k}(\mathbf{x}, t|\mathbf{x}', t') \frac{\mathrm{d}\psi(\overline{S})}{\mathrm{d}\overline{S}(\mathbf{x}', t')} \right] \overline{\mathbf{s}}(\mathbf{x}', t') = 0. \tag{D1}$$

[67] Multiplying (D1) with x_i and integrating over space gives an equation for the center of mass in the i direction,

$$\frac{\partial m_i^{(1)}(t)}{\partial t} = -\mathbf{q}(t) \cdot A^{-1} \int \mathrm{d}^d x \nabla \psi[\overline{S}(\mathbf{x}, t)]. \tag{D2}$$

Here the mean flow and pressure fluctuations are aligned with the 1 direction so that we obtain

$$\frac{\partial m_i^{(1)}(t)}{\partial t} = -\delta_{i1} q(t) \cdot A^{-1} \int \mathrm{d}^d x \frac{\partial}{\partial x_1} \psi[\overline{S}(\mathbf{x}, t)] = \delta_{i1} q(t) A^{-1} \int \mathrm{d}^{d-1} y \psi[\overline{S}(x = 0, y, t)] = \delta_{i1} q(t), \tag{D3}$$

where we have used the boundary condition $\overline{S}(\mathbf{x}, t)|_{x1=0} = 1$ and the definition of the fractional flow function (8). Relation (D3) expresses mass conservation of the injected fluid.

[68] Analogously, multiplying (D1) with x_1^2 and integrating over space gives an equation for the longitudinal second moment,

$$\frac{\partial m_{11}^{(2)}(t)}{\partial t} = 2q(t) \cdot A^{-1} \int \mathrm{d}^d x \psi[\overline{S}(\mathbf{x}, t)] - 2A^{-1} \int \mathrm{d}^d x \int_0^t \mathrm{d}t' \int \mathrm{d}^d x' \frac{\mathrm{d}\psi(\overline{S})}{\mathrm{d}\overline{S}(\mathbf{x}, t)} k_{1j}(\mathbf{x}, t|\mathbf{x}', t') \cdot \frac{\partial}{\partial x_j'} \psi[\overline{S}(x', t')]. \tag{D4}$$

Thus, the growth of the width of the saturation distribution is given by

$$\frac{\partial \kappa_{11}(t)}{\partial t} = q(t) \left[2A^{-1} \int \mathrm{d}^d x \psi[\overline{S}(\mathbf{x}, t)] - \int_0^t \mathrm{d}t' q(t') \right] - 2A^{-1} \int \mathrm{d}^d x \int_0^t \mathrm{d}t' \int \mathrm{d}^d x' \frac{\mathrm{d}\psi(\overline{S})}{\mathrm{d}\overline{S}(\mathbf{x}, t)} k_{1j}(\mathbf{x}, t|\mathbf{x}', t') \cdot \frac{\partial}{\partial x_j'} \psi[\overline{S}(x', t')]. \tag{D5}$$

Appendix E: Dispersion Coefficient

[69] Starting from (39) we execute the x_1-integration, yielding

$$d_{11}^s(t) = -\sigma_{ff}^2 \int_0^t \mathrm{d}t' \int_0^\infty \mathrm{d}x_1' \frac{x_1'}{x_1(t')} C_{11} \left\{ \frac{x_1'}{x_1(t')} [x_1(t) - x_1(t')] \right\} \times q(t) q(t') \frac{\partial}{\partial x_1'} \psi \left\{ S_0 \left[\frac{x_1'}{x_f(t')} \right] \right\}. \tag{E1}$$

After rescaling x'_1 with $x_1(t')$ we obtain

$$d_{11}^s(t) = -\sigma_{ff}^2 \int_0^t \mathrm{d}t' \int_0^\infty \mathrm{d}x_1' x_1' C_{11} \{ x_1' [x_1(t) - x_1(t')] \} \times q(t) q(t') \frac{\partial}{\partial x_1'} \psi \{ S_0 [x_1'/C] \}, \tag{E2}$$

where $C = \mathrm{d}\psi(S^f)/\mathrm{d}S^f$. Changing variables from t' to $x_1(t')$ ($\mathrm{d}t' = q(t')^{-1}\,\mathrm{d}x_1(t')$) gives

$$d_{11}^s(t) = -\sigma_{ff}^2 \int_0^{x_1(t)} \mathrm{d}x_1 \int_0^{\infty} \mathrm{d}x_1' x_1' C_{11}\{x_1'[x_1(t) - x_1]\} \times q(t) \frac{\partial}{\partial x_1'} \psi\{S_0[x_1'/C]\}. \tag{E3}$$

Shifting x_1 by $x_1(t)$ and subsequent rescaling with x_1' gives

$$d_{11}^s(t) = -\sigma_{ff}^2 \int_0^{x_1(t)} \mathrm{d}x_1 \int_0^{\infty} \mathrm{d}x_1' C_{11}(x_1) q(t) \frac{\partial}{\partial x_1'} \psi\{S_0[x_1'/C]\}. \tag{E4}$$

And finally after executing the x_1' integration we obtain

$$d_{11}^s(t) = \sigma_{ff}^2 q(t) \int_0^{x_1(t)} \mathrm{d}x_1 C_{11}(x_1). \tag{E5}$$

We now expand the integral for $x_1(t) = qt + \int_0^t \mathrm{d}t' q'(t')$, which gives in lowest order

$$d_{11}^s(t) = \sigma_{ff}^2 q(t) \left[\int_0^{qt} \mathrm{d}x_1 C_{11}(x_1) + \int_0^t \mathrm{d}t' q'(t') C_{11}(qt) \right]. \tag{E6}$$

Appendix F: Alternative Measures for Front Spreading

[70] *Neuweiler et al.* [2003] defined a macrodispersion coefficient by looking at Fickian analogues to the (nonlocal) dispersive flux resulting from the upscaling exercise in section 3.1:

$$\mathbf{j}(\mathbf{x}, t) = \int_{\mathbf{0}}^t \mathrm{d}t' \int \mathrm{d}^d x' \frac{\mathrm{d}\psi(\overline{S})}{\mathrm{d}\overline{S}(\mathbf{x}, t)} \mathbf{k}(x, t|x', t') \nabla' \psi[\overline{S}(\mathbf{x}', t')]. \tag{F1}$$

[71] A macrodispersion coefficient according to *Neuweiler et al.* [2003] is then defined by setting

$$j_i(\mathbf{x}, t) \equiv d_{ij}^{\psi}(t) \frac{\partial}{\partial x_j} \psi[\overline{S}(\mathbf{x}, t)]. \tag{F2}$$

[72] The macrodispersion coefficients are obtained by multiplying (F2) by x_j and integration of the resulting expression over space. This gives

$$d_{ij}^{\psi}(t) = \left\{ \int \mathrm{d}^d x \psi[\overline{S}(\mathbf{x}, t)] \right\}^{-1} \times \int \mathrm{d}^d x \int_0^t \mathrm{d}t' \int \mathrm{d}^d x' x_j \frac{\mathrm{d}\psi(\overline{S})}{\mathrm{d}\overline{S}(\mathbf{x}, t)} k_{il}(\mathbf{x}, t|\mathbf{x}', t') \cdot \frac{\partial}{\partial x_l'} \psi[\overline{S}(x', t')]. \tag{F3}$$

[73] This definition is identical to the one used by *Neuweiler et al.* [2003]. In lowest-order erturbation theory, we obtain for the denominator

$$A \int \mathrm{d}x_1 \psi\left\{ S_0\left[\frac{x_1}{C x_1(t)}\right] \right\} = AB x_1(t), \tag{F4}$$

where we define

$$B \equiv C \int \mathrm{d}^d x \psi[S_0(x_1)]. \tag{F5}$$

[74] Thus, we get for the macrodispersion coefficient in lowest-order perturbation theory

$$d_{11}^{\psi}(t) = -\frac{\sigma_{ff}^2}{B x_1(t)} \int \mathrm{d}x_1 \int_0^t \mathrm{d}t' \int_0^{\infty} \mathrm{d}x_1' \frac{x_1^2}{x_1(t)} C_{11}(x_1 - x_1') q(t) q(t') \times \frac{1}{x_1(t)} \delta\left[\frac{x_1'}{x_1(t')} - \frac{x_1}{x_1(t)}\right] \frac{\partial}{\partial x_1'} \psi\left\{ S_0\left[\frac{x_1'}{x_f(t')}\right] \right\}, \tag{F6}$$

where we used expression (C1) for $\mathrm{d}\psi(S_0)/\mathrm{d}S_0$. Executing the x_1 integration yields

$$d_{11}^{\psi}(t) = -\frac{\sigma_{ff}^2}{B} \int_0^t \mathrm{d}t' \int_0^{\infty} \mathrm{d}x_1' \frac{{x_1'}^2}{x_1(t')^2} C_{11}\left\{ \frac{x_1'}{x_1(t')}[x_1(t) - x_1(t')] \right\} \times q(t) q(t') \frac{\partial}{\partial x_1'} \psi\left\{ S_0\left[\frac{x_1'}{x_f(t')}\right] \right\}. \tag{F7}$$

[75] After rescaling x'_1 with $x_1(t')$ we obtain

$$d_{11}^{\psi}(t) = -\frac{\sigma_{ff}^2}{B} \int_0^t \mathrm{d}t' \int_0^{\infty} \mathrm{d}x_1' {x_1'}^2 C_{11}\{x_1'[x_1(t) - x_1(t')]\} \times q(t) q(t') \frac{\partial}{\partial x_1'} \psi\{S_0[x_1'/C]\}, \tag{F8}$$

where $C = \mathrm{d}\psi(S^f)/\mathrm{d}S^f$. Changing variables from t' to $x_1(t')$ ($\mathrm{d}t' = q(t')^{-1}\,\mathrm{d}x_1(t')$) gives

$$d_{11}^{\psi}(t) = -\frac{\sigma_{ff}^2}{B} \int_0^{x_1(t)} \mathrm{d}x_1 \int_0^{\infty} \mathrm{d}x_1' {x_1'}^2 q(t) C_{11}\{x_1'[x_1(t) - x_1]\} \times \frac{\partial}{\partial x_1'} \psi\{S_0[x_1'/C]\}. \tag{F9}$$

Shifting x_1 by $x_1(t)$ and subsequent rescaling with x'_1 gives

$$d_{11}^{\psi}(t) = -\frac{\sigma_{ff}^2}{B} \int_0^{x_1(t)} \mathrm{d}x_1 \int_0^{\infty} \mathrm{d}x_1' x_1' q(t) C_{11}(x_1) \frac{\partial}{\partial x_1'} \psi\{S_0[x_1'/C]\}. \tag{F10}$$

[76] And finally we obtain after integration by parts

$$d_{11}^{\psi}(t) = \sigma_{ff}^2 q(t) \int_0^{x_1(t)} \mathrm{d}x_1 C_{11}(x_1), \tag{F11}$$

which is identical to the expression obtained from the moment equations. Following *Neuweiler et al.* [2003], we insert $C_{11}(x_1) = l\delta(x_1)$ and obtain

$$d_{11}^{\psi}(t) = \sigma_{ff}^2 l q(t). \tag{F12}$$

[77] Thus, on average, there is no contribution to the macrodispersion coefficient due to temporal fluctuations.

[78] *Langlo and Espedal* [1995] used a more process-oriented definition for the macrodispersion coefficient in terms of the dispersive flux term in (29). Assuming that $\mathbf{k}(\mathbf{x}, t|\mathbf{x}', t')$ is sharply peaked about $\mathbf{x}$ and t, the flux term in (29) can be localized in space and time, which yields

$$\frac{\partial \overline{S}(\mathbf{x},t)}{\partial t} + \mathbf{q}(t)\cdot\nabla\psi(\overline{S}) - \nabla\cdot\frac{\mathrm{d}\psi(\overline{S})}{\mathrm{d}\overline{S}}\mathbf{d}(\mathbf{x},t)\frac{\mathrm{d}\psi(\overline{S})}{\mathrm{d}\overline{S}}\nabla\overline{S}(\mathbf{x},t) = 0, \tag{F13}$$

where we defined

$$\mathbf{d}(\mathbf{x},t) = \int_{\mathbf{0}}^{t}\mathrm{d}t'\int \mathrm{d}^d x'\mathbf{k}(x,t|x',t'). \tag{F14}$$

The latter is similar to the macrodispersion coefficient as identified by *Langlo and Espedal* [1995].

Appendix G: Spatially Homogeneous Medium

[79] Here we consider flow in spatially homogeneous medium under temporal pressure fluctuations. We demonstrate an artificial dispersion effect due to temporal pressure fluctuations when considering the moments of the time averaged saturation and analyze the purely advective widening of the saturation distribution behind the front.

[80] As given in section 3.3, we determine the width of the saturation distribution in a homogeneous medium in terms of the moments of

$$s_1^{(0)}(x_1,t) = -A^{-1}\frac{\partial}{\partial x_1}S_0(x_1,t). \tag{G1}$$

We immediately obtain for the first moment of $s^{(0)}(x_1, t)$

$$m_1^{(1)}(t) = \int_0^t \mathrm{d}t' q(t') \tag{G2}$$

as a consequence of mass conservation. The second moment is given by

$$\frac{\mathrm{d}m_{11}^{(2)}(t)}{\mathrm{d}t} = 2q(t)\int \mathrm{d}^d x_1 \psi[S_0(x_1,t)]. \tag{G3}$$

[81] The saturation $S_0(x_1, t)$ in a homogeneous medium has a sharp front. It is given by (11). Thus, (G3) assumes the form

$$m_{11}^{(2)}(t) = \frac{\mathrm{d}\psi(S^f)}{\mathrm{d}S^f}\left[\int_0^t \mathrm{d}t' q(t')\right]^2 \int_0^1 \mathrm{d}x_1 \psi[S^r(x_1)]. \tag{G4}$$

G1. Average Width of Saturation

[82] We obtain for the width $\kappa_{11}(t)$ in a single realization of the pressure fluctuations

$$\kappa_{11}(t) = \left[\int_0^t \mathrm{d}t' q(t')\right]^2\left[\frac{\mathrm{d}\psi(S^f)}{\mathrm{d}S^f}\int_0^1 \mathrm{d}x_1\psi[S^r(x_1)] - 1\right]. \tag{G5}$$

The latter, however, is not related to actual spreading of the saturation front. The spread of the saturation front is quantified by the second term on the right side of (D4).

[83] The (temporal) ensemble average of the latter is given by

$$\langle\kappa_{11}(t)\rangle = \left[(qt)^2 + \int_0^t \mathrm{d}t'\int_0^t \mathrm{d}t''\langle q'(t')q'(t'')\rangle\right] \times\left[\frac{\mathrm{d}\psi(S^f)}{\mathrm{d}S^f}\int_0^1 \mathrm{d}x_1\psi[S^r(x_1)] - 1\right]. \tag{G6}$$

The fluctuation-induced contribution measures the uncertainty of the front position in the homogeneous medium from realization to the realization of the pressure fluctuations, see Figure 3. It does not contribute to the spreading of the saturation front.

G2. Width of the Average Saturation

[84] The width of the average saturation front is given by the ensemble second centered moment

$$\kappa_{11}^{\mathrm{ens}}(t) = \left\langle m_{11}^{(2)}(t)\right\rangle - \left\langle m_1^{(1)}(t)\right\rangle^2. \tag{G7}$$

We obtain for $\kappa_{11}^{\mathrm{ens}}$ by using (G4) and (G2)

$$\kappa_{11}^{\mathrm{ens}}(t) = \langle\kappa_{11}(t)\rangle + \int_0^t \mathrm{d}t'\int_0^t \mathrm{d}t''\langle q'(t')q'(t'')\rangle. \tag{G8}$$

Thus, the second centered moment of the average saturation quantifies a purely advective spreading effect due to temporal fluctuations of the front position that are suppressed in (G6), which measures the advective widening of the saturation distribution behind the front.

[85] **Acknowledgments.** The authors would also like to thank the "CIUDEN" initiative for their financial contribution to this work. Additionally, D.B. and M.D. gratefully acknowledge the financial support of the Spanish Ministry of Science and Innovation (MCI) through the "Juan de la Cierva" and "Ramón y Cajal" programs.

References

Abramowitz, M., and I. Stegun (1970), *Handbook of Mathematical Functions*, Dover, New York.

Bachu, S. (2000), Sequestration of CO_2 in geological media: Criteria and approach for site selection in response to climate change, *Energy Convers. Manage.*, *41*(9), 953–970, doi:10.1016/S0196-8904(99)00149-1.

Bear, J. (1972), *Dynamics of Fluids in Porous Media*, Elsevier, New York.

Blunt, M. J., J. W. Barker, B. Rublin, M. Mansfeld, I. Culverwell, and M. Christie (1994), Predictive theory for viscous fingering in compositional displacement, *SPE Reservoir Eng.*, *36*, 73–80.

Cirpka, O. A., and S. Attinger (2003), Effective dispersion in heterogeneous media under random transient flow conditions, *Water Resour. Res.*, *39*(9), 1257, doi:10.1029/2002WR001931.

Cushman, J. H., X. Hu, and T. R. Ginn (1994), Nonequilibrium statistical mechanics of preasymptotic dispersion, *J. Stat. Phys.*, *75*(5–6), 859–878.

Cvetkovic, V., and G. Dagan (1996), Reactive transport and immiscible flow in geological media. II. Applications, *Proc. R. Soc. London, Ser. A*, *452*, 303–328.

Dagan, G. (1989), *Flow and Transport in Porous Formations*, Springer, New York.

Dentz, M., and J. Carrera (2003), Effective dispersion in temporally fluctuating flow through a heterogeneous medium, *Phys. Rev. E*, *68*, 036310, doi:10.1103/PhysRevE.68.036310.

Dentz, M., and J. Carrera (2005), Effective solute transport in temporally fluctuating flow through heterogeneous media, *Water Resour. Res.*, *41*, W08414, doi:10.1029/2004WR003571.

Dentz, M., H. Kinzelbach, S. Attinger, and W. Kinzelbach (2000), Temporal behavior of a solute cloud in a heterogeneous porous medium: 1. Point-like injection, *Water Resour. Res*, *36*(12), 3591–3604.

Efendiev, Y., and L. J. Durlofsky (2002), Numerical modeling of subgrid heterogeneity in two phase flow simulations, *Water Resour. Res.*, *38*(8), 1128, doi:10.1029/2000WR000190.

Fiori, A. (2001), On the influence of local dispersion in solute transport through formations with evolving scales of heterogeneity, *Water Resour. Res.*, *37*(2), 235–242.

Gelhar, L. (1993), *Stochastic Subsurface Hydrology*, Prentice Hall, Englewood Cliffs, N. J.

Gelhar, L., and C. Axness (1983), Three-dimensional stochastic analysis of macrodispersion in aquifers, *Water Resour. Res.*, *19*(1), 161–180.

Hasle, G., K.-A. Lie, and E. Quak (2007), *Geometric Modelling, Numerical Simulation, and Optimization*, Springer, Berlin.

Jarman, K. D., and T. F. Russell (2003), Eulerian moment equation for 2-D stochastic immiscible flow, *Multiscale Modeling Simul.*, *1*, 598–608.

Jarman, K. D., and A. M. Tartakovsky (2008), Divergence of solutions to solute transport moment equations, *Geophys. Res. Lett.*, *35*, L15401, doi:10.1029/2008GL034495.

Kinzelbach, W., and P. Ackerer (1986), Modélisation du transport de contaminant dans un champ d'écoulement non-permanent, *Hydrogeologie*, *2*, 197–205.

Kitanidis, P. K. (1988), Prediction by the method of moments of transport in heterogeneous formations, *J. Hydrol.*, *102*, 453–473.

Koch, D. L., and J. F. Brady (1987), A non-local description of advection-diffusion with application to dispersion in porous media, *J. Fluid Mech.*, *180*, 387–403.

Kubo, R., M. Toda, and N. Hashitsume (1991), *Statistical Physics II, Non-Equilibrium Statistical Mechanics*, Springer, Berlin.

Lake, L. (1989), *Enhanced Oil Recovery*, Prentice Hall, Englewoods Cliffs, N. J.

Langlo, P., and M. Espedal (1995), Macrodispersion for two-phase, immiscible flow in porous media, *Adv. Water Resour.*, *17*, 297–316.

Marle, C. M. (1981), *Multiphase Flow in Porous Media*, Inst. Fr. du Pet, Paris.

Morales-Casique, E., S. P. Neuman, and A. Guadagnini (2006), Non-local and localized analyses of non-reactive solute transport in bounded randomly heterogeneous porous media: Computational analysis, *Adv. Water Resour.*, *29*, 1399–1418.

Neuman, S. P. (1993), Eulerian-Lagrangian theory of transport in space-time nonstationary velocity fields: Exact nonlocal formalism by conditional moments and weak approximation, *Water Resour. Res.*, *29*(3), 633–645.

Neuweiler, I., S. Attinger, W. Kinzelbach, and P. King (2003), Large scale mixing for immiscible displacement in heterogenous porous media, *Transp. Porous Media*, *51*, 287–314.

Noetinger, B., V. Artus, and L. Ricard (2004), Dynamics of the water-oil front for two-phase, immiscible flow in heterogeneous porous media. 2. Isotropic media, *Transp. Porous Media*, *56*, 305–328.

Pop, I. S., and B. Schweizer (2007), On the homogenization of the Buckley-Leverett equation including trapping effects at the micro scale, *Proc. Appl. Math. Mech.*, *7*, 1,024,701–1,024,702.

Rehfeldt, K. R., and L. W. Gelhar (1992), Stochastic analysis of dispersion in unsteady flow in heterogeneous aquifers, *Water Resour. Res.*, *28*(8), 2085–2099.

Saffman, P. G., and G. I. Taylor (1958), The penetration of a fluid into a porous medium or Hele-Shaw cell containing a more viscous liquid, *Proc. R. Soc. London, Ser. A*, *245*, 312–329.

Tartakovsky, A. M., S. P. Neuman, and R. J. Lenhard (2003), Immiscible front evolution in randomly heterogeneous porous media, *Phys. Fluids*, *15*, 3331–3341.

Tartakovsky, D. M., and S. P. Neuman (1998a), Transient flow in bounded randomly heterogeneous domains: 1. Exact conditional moment equations and recursive approximations, *Water Resour. Res.*, *34*(1), 1–12.

Tartakovsky, D. M., and S. P. Neuman (1998b), Transient effective hydraulic conductivities under slowly and rapidly varying mean gradients in bounded three-dimensional random media, *Water Resour. Res.*, *34*(1), 21–32.

Zwanzig, R. (1961), Memory effects in irreversible thermodynamics, *Phys. Rev.*, *124*, 983–992.

D. Bolster and M. Dentz, Department of Geotechnical Engineering and Geosciences, Technical University of Catalonia, E-08034 Barcelona, Spain. (diogobolster@gmail.com)

J. Carrera, Institute of Environmental Analysis and Water Studies, CSIC, Barcelona E-08034, Spain.